Journal of Molecular Catalysis A: Chemical 312 (2009) 18–22

Contents lists available at ScienceDirect

Journal of Molecular Catalysis A: Chemical

journal homepage: www.elsevier.com/locate/molcata

Cobalt ferrite aerogels by epoxide sol–gel addition: Efficient catalysts for the hydrolysis of 4-nitrophenyl phosphate

Joelle Akl[a], Tarek Ghaddar[a], Aline Ghanem[b], Houssam El-Rassy[a,*]

[a] Department of Chemistry, American University of Beirut, P.O. Box 11-0236, Riad El-Solh 1107 2020, Beirut, Lebanon
[b] Department of Chemistry, Lebanese University, Faculty of Sciences II, P.O. Box 90-656 Jdeidet El-Matn, Lebanon

ARTICLE INFO

Article history:
Received 8 April 2009
Received in revised form 17 June 2009
Accepted 23 June 2009
Available online 2 July 2009

Keywords:
Cobalt ferrite
Aerogel
Sol–gel
Catalysis
4-Nitrophenyl phosphate hydrolysis

ABSTRACT

Porous cobalt ferrite aerogel catalysts were obtained by 1,2-epoxide sol–gel process and investigated in the hydrolysis of 4-nitrophenyl phosphate. These materials were synthesized by reacting cobalt and iron salts with propylene oxide in methanol, dried by supercritical carbon dioxide, and calcined between 200 and 800 °C. The catalysts were characterized using Fourier Transform Infrared (FTIR) spectroscopy, nitrogen adsorption–desorption technique, and powder X-ray diffraction (XRD). The "as-prepared aerogel" surface exhibits M–OH groups that disappear after annealing, which enhances the spinel structure. This was coupled with a better crystallinity revealed by XRD peaks sharpness. The crystallite sizes were found to be between 6.3 and 28.1 nm. In addition, the catalysts revealed high porosities that decrease as the annealing temperature increases. The catalysis showed that the catalytic activity significantly rely on the synthesis procedure and mainly the calcination temperature. Samples calcined at 600 °C and above did not show any catalytic activity, however, the highest catalytic efficiency was for those calcined at 200 °C with 100% selectivity for the 4-nitrophenol. The correlation of the characterization techniques and the catalysis tests revealed that the catalytic properties of these sol–gel materials are due to the existence of residual surface OH groups.

1. Introduction

Transition metal ferrites are the most widely used magnetic materials [1] that exhibit chemical stability, low electric loss, high coercivity and thus interesting magnetic properties. In addition to their application in microwave devices, computer memories and magnetic storage [2], these materials of type $M^{II}Fe^{III}{}_2O_4$ have been recently used in heterogeneous catalysis applied to various organic reactions. For instance, the catalytic activity of such solids was studied in: conversion of isopropanol to propene and acetone [3], thermal decomposition of ammonium perchlorate [4], oxidative dehydrogenation of *n*-butene [5,6], production of orthoalkylphenol [7], decomposition of cyclohexanol [8], and selective mono-N-methylation of aniline [9].

Among others, cobalt ferrite ($Co^{II}Fe^{III}{}_2O_4$) is one of these transition metal ferrites that were used in catalysis [7,8]. It has a face-centered cubic structure composed of large unit cells, containing eight formula units [10]. During the last decade, numerous techniques were explored for the synthesis of uniform cobalt ferrite including pulse laser deposition [11], electrodeposition [12], wet chemical method [13], coprecipitation [14], hydrothermal synthesis [15], mechano-synthesis [16], combustion [17], organic precursor decomposition [18,19], and sol–gel processes [20–23]. In addition to the pure cobalt ferrite, other metal-cobalt ferrites were successfully prepared starting from various mixtures of metal precursors [7,8].

Previously developed sol–gel [24] techniques for the synthesis of cobalt ferrite used either a mixture of the metal nitrate salt with a citric acid solution [20,22,23], or a mixture of metal alkoxides [21]. A well known drying technique for sol–gel materials is the supercritical drying, where the liquid wetting the solid network is exchanged with another fluid brought to a hypercritical state before its evacuation [25]. This technique, leading to the so-called "aerogels", largely attenuates the capillary stress responsible of the gel network compression, its shrinkage and its porosity loss [26].

Some oxide aerogels were recently prepared via the epoxide addition sol–gel method, where the reaction between the metal salt and propylene oxide in alcohol led to a sol that was transformed to a gel and dried under supercritical carbon dioxide [27–29]. This technique successfully generated oxides exhibiting high porosity and specific surface area, and therefore materials that might have significant impacts in catalysis.

We report in the present study, for the first time to our knowledge, the synthesis of a highly porous bi-metallic cobalt ferrite $Co^{II}Fe^{III}{}_2O_4$ aerogels according to the epoxide sol–gel addition technique derived from Gao et al. [28]. These aerogels were calcined

* Corresponding author. Tel.: +961 1 350000x4051; fax: +961 1 365217.
E-mail address: Houssam.Rassy@aub.edu.lb (H. El-Rassy).

1381-1169/$ – see front matter © 2009 Elsevier B.V. All rights reserved.
doi:10.1016/j.molcata.2009.06.026

at different temperatures and used in heterogeneous liquid–solid catalysis of the hydrolysis of 4-nitrophenyl phosphate.

2. Experimental

2.1. Materials

The chemicals were used in this study as received and without further purification. Cobalt (II) chloride hexahydrate was provided by AnalaR. Iron (III) chloride hexahydrate was from Fluka. Propylene oxide, 4-nitrophenyl phosphate disodium salt (4-NPP), 4-nitrophenol (4-NP), and glycine were purchased from Acros Organics. Methanol was supplied by Sigma–Aldrich. $NaH_2PO_4{\cdot}H_2O$ and Na_2HPO_4 used for the preparation of the phosphate buffer solution (PBS, pH 7.0, 10 mM) were from Merck, and sodium hydroxide from Himedia.

2.2. Catalyst preparation

Cobalt ferrite aerogels were prepared in polypropylene vials by dissolving 79.3 mg (0.33 mmol) of $CoCl_2{\cdot}6H_2O$ and 180.2 mg (0.67 mmol) of $FeCl_3{\cdot}6H_2O$ in 3 mL of methanol under vigorous stirring. To the obtained solution, 700 μL (10 mmol) of propylene oxide were added. The stirring was stopped after a few minutes and the solution was kept at rest for gelation, which was observed in the next 20–25 min. The obtained gel was kept for one day at room temperature for aging, followed by a drying under supercritical carbon dioxide (T_C = 31.1 °C; P_C = 73.7 bar) leading to the final aerogel, noted A-$CoFe_2O_4$-RT (*i.e.* cobalt ferrite aerogel at room temperature). This terminal step was preceded by a 24 h solvent exchange step, where the residual solvent in the gel was exchanged by acetone presenting a higher miscibility with liquid carbon dioxide. A-$CoFe_2O_4$-RT samples were calcined in a muffle furnace under air at temperatures between 200 and 800 °C with a heating ramp rate of 1 °C/min. The temperature was maintained at the desired temperature for 5 h before cooling.

2.3. Catalyst characterization

Nitrogen sorption technique was used for the determination of the textural properties of the obtained materials. For that purpose, a Nova 2200e high-speed surface area and pore size analyzer (Quantachrome Instruments) was used. Prior to the measurement, the aerogel samples were degassed for 2 h at room temperature. The specific surface area was calculated according to the BET theory [30], while the pore size distribution and the pore volume were calculated by the BJH method [31] based on the desorption branch of the isotherm. FTIR spectra were collected on a Thermo Nicolet 4700 Fourier Transform Infrared Spectrometer equipped with a Class 1 Laser. The measurements were performed using the transmission KBr pellet technique, where 0.5% in weight aerogel powder-containing potassium bromide pellets were used. Powder X-ray diffraction patterns were recorded on a Bruker d8 discover X-ray diffractrometer equipped with a Cu-Kα radiation (λ = 1.5405 Å).

2.4. Catalytic activity

To determine the activity of these catalysts, the hydrolysis of 4-nitrophenyl phosphate to produce 4-nitrophenol has been chosen as a model reaction. In a 40-mL reactor, operating at 30 °C under atmospheric pressure and magnetic stirring, 5×10^{-5} mmol of 4-nitrophenyl phosphate were dissolved in 25 mL of 50 mM aqueous glycine–NaOH buffer solution (pH 9.5) to make a 2 mM initial concentration. To these solutions, 50 mg of each catalyst were added. Aliquots were taken at different time intervals and filtered on Millex-LG 4 mm 0.2 μm PTFE filters (from Millipore). Samples were analyzed by HPLC with a diode array UV detector (Agilent 1100 series) on a Discovery HS C_{18} column (250 mm × 4.6 mm, 5 μm particles, from Supelco) at room temperature (20–22 °C). The eluent composition was 40/60 methanol/PBS at a flow-rate of 1 mL min^{-1}. 4-NPP was detected at 311 nm while 4-NP was detected at 404 nm. The retention times for the 4-NPP and 4-NP were 2.7 and 7.6 min, respectively.

3. Results and discussion

3.1. Synthesis

The synthesis resulted in a low-density clear brown aerogel exhibiting a density around 0.06 g/cm^3. The density has been calculated by dividing the mass of the aerogel by its volume immediately after the supercritical drying. This gel was very soft and breaks down into fine powder easily. A noticeable change in the solution color has been observed during the gel preparation, where a conversion of the alcoholic metals solution color from clear brown to dark brown has been observed immediately after the addition of the propylene oxide. This color persists unchanged until the solution viscosity increases, which was coupled with a gradual change of the color to clear brown, 2 min before the complete gelation occurs. The hexaaquacobalt (II) and hexaaquairon (III) ions are the acids that react with the propylene oxide playing the role of a base leading to the deprotonation of the metal hydrate and the protonation of the epoxide. This step is followed by an irreversible epoxide ring opening due to a nucleophilic attack by the counterions that generates 1-chloro-2-propanol [27]. In a second step, the aqua-hydroxy deprotonated species $[Co(OH)(H_2O)_5]^+$ and $[Fe(OH)(H_2O)_5]^{2+}$ undergo condensation reactions of olation and oxolation to yield oligomeric species [32]. In these oxo-bridged M–O–M′ groups, M and M′ are two cobalt, two iron, or one cobalt and one iron atoms. The remaining aqua-ligands react similarly with propylene oxide molecules to form other M–O–M′ groups. Carbon dioxide supercritical drying has been used and yielded the A-$CoFe_2O_4$-RT. The heat treatment of this latter revealed a change of the material color coupled with a modification of its porosity and crystalline structure. Calcined samples are noted as follows: A-$CoFe_2O_4$-200 (*i.e.* cobalt ferrite aerogel calcined at 200 °C); A-$CoFe_2O_4$-300; A-$CoFe_2O_4$-400; A-$CoFe_2O_4$-500; A-$CoFe_2O_4$-600; A-$CoFe_2O_4$-700; A-$CoFe_2O_4$-800.

3.2. Catalyst characterization

In addition to the results shown in Fig. 1, absorption bands centered at 3422 and 1636 cm^{-1} are seen for the calcined and non-calcined aerogels, and are attributed to the residual coordinated or adsorbed water molecules [33]. Moreover, A-$CoFe_2O_4$-RT exhibits several bands attributed to the residual 1-chloro-2-propanol. Bands in the 3000–2800 cm^{-1} range are easily attributed to the C–H symmetric and antisymmetric stretching vibrations, and others appearing at 1484, 1391 and 1377 cm^{-1} are assigned to the C–H antisymmetric and symmetric deformation vibrations, respectively [34]. The FTIR absorption spectra of the obtained sol–gel materials revealed a difference in the existing chemical groups for the different aerogels, mainly in the range between 1200 and 400 cm^{-1} (Fig. 1). The band at 1045 cm^{-1} corresponds to the C–O stretching vibration [33]. Besides these peaks, A-$CoFe_2O_4$-RT shows two bands at 655–630 and 472 cm^{-1} that are attributed to the M–OH deformation vibration and M–O stretching vibration, respectively [35]. The existence of the broad band at 655–630 cm^{-1} reflects the subsistence of residual Co–OH and Fe–OH groups on the surface of the network that did not undergo the condensation. The spectra of the calcined aerogels reveal the formation of tetrahedral metal-oxygen groups reflected by the appearance of a band at 586 cm^{-1} that corresponds to the M–O stretching vibration mode in ferrites

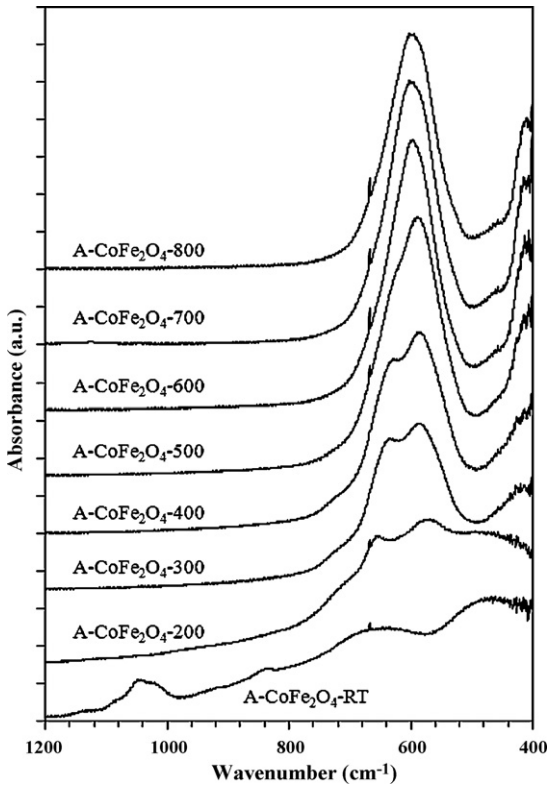

Fig. 1. FTIR absorption spectra of prepared cobalt ferrite aerogels.

[36,37]. It is important to note that the intensity of the band at 655–630 cm^{-1} corresponding to residual M–OH decreases when the calcination temperature increases, and disappears above 600 °C. This decrease was coupled with an increase of the M–O stretching vibration bands at 586 cm^{-1}. The very sharp peak appearing at 668 cm^{-1} is attributed to the M–O stretching vibrations [38].

Powder X-ray diffraction (XRD) patterns did not show any crystalline structure for the A-$CoFe_2O_4$-RT, however, clear peaks appeared after heat treatment (Fig. 2). These peaks became very sharp at high calcination temperatures and could be indexed in a simple cubic lattice. The peaks positions as well as their relative intensities match perfectly the $CoFe_2O_4$ powder diffraction data (JCPDS 22-1086). The average size of the crystallites calculated from the broadening of the highest intensity XRD peak (3 1 1) using the Scherrer equation [39] increased from 6.26 nm for the A-$CoFe_2O_4$-300 to 28.10 nm for the A-$CoFe_2O_4$-800 (Table 1), confirming the nanoparticle nature of these cobalt ferrite samples. The very weak peaks in the XRD pattern of the A-$CoFe_2O_4$-200, as well as the absence of clear peaks for the A-$CoFe_2O_4$-RT are therefore due to the extremely small cobalt ferrite crystallite size that makes these peaks uneasily distinguished.

Table 1
Average crystallite size (ACS), specific surface area (SSA), percentage of specific surface area above the Kelvin limit (SSA_{kel}), total pore volume (V_p) and percentage of pore volume above the Kelvin limit ($V_{p,kel}$), calculated for the prepared cobalt ferrite aerogels.

	ACS (nm)	SSA (m^2/g)	SSA_{kel} (%)	V_p (cm^3/g)	$V_{p,kel}$ (%)
A-$CoFe_2O_4$-RT	–	576	84	1.31	89
A-$CoFe_2O_4$-200	–	223	>99	0.76	>99
A-$CoFe_2O_4$-300	6.26	115	95	0.55	99
A-$CoFe_2O_4$-400	9.80	93	94	0.54	98
A-$CoFe_2O_4$-500	13.03	53	94	0.31	97
A-$CoFe_2O_4$-600	20.03	26	89	0.07	91
A-$CoFe_2O_4$-700	25.82	13	89	0.03	88
A-$CoFe_2O_4$-800	28.10	13	94	0.03	86

The nitrogen adsorption isotherms of the A-$CoFe_2O_4$-RT revealed a type IV isotherm [40] with a hysteresis loop, having a specific surface area equal to 576 m^2/g and a pore volume 1.31 g/cm^3. Calculations revealed that this aerogel has mainly mesopores (between 2 and 50 nm) with the existence of micropores (smaller than 2 nm) not exceeding 16% of the totality of the pores. It was noticed also that the surface area and pore volume decreases after the heat treatment of the aerogels, with a drastic decrease after 600 °C. This is correlated with the aerogel sintering leading to the increase of the crystallite size and the decrease of the voids between the particles. Detailed results are regrouped in Table 1.

The correlation between the FTIR, XRD, and nitrogen adsorption results confirm the formation of cobalt ferrite mesoporous aerogel nanoparticles having considerable surface area and porosity, mainly at room temperature and after calcinations between 200 and 500 °C.

3.3. Catalytic activity

In addition to their catalytic properties, these ferrites showed a very fast adsorption capacity for the 4-NPP. This was noticed since the concentration of the 4-NPP in the reaction medium has

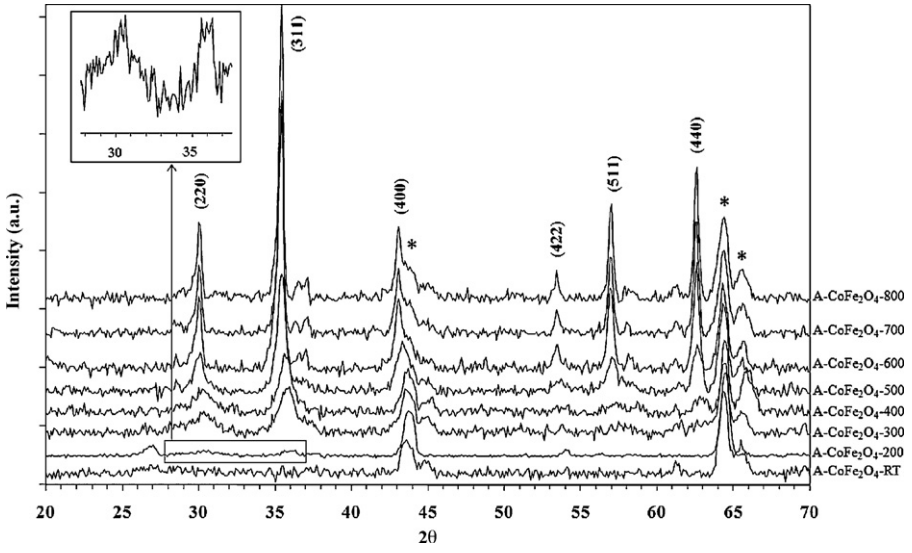

Fig. 2. XRD patterns of prepared cobalt ferrite aerogels. Peaks marked with a star correspond to the used sample holder.

Table 2
Catalytic activities of the prepared cobalt ferrite aerogels for the hydrolysis of 4-nitrophenyl phosphate.

	4-NPP conversion after 5 h (%)	4-NPP conversion after 24 h (%)	Initial rate (mmol L^{-1} min^{-1})	Rate constant (min^{-1})
A-$CoFe_2O_4$-RT	19.06	55.37	2.50×10^{-3}	2.67×10^{-3}
A-$CoFe_2O_4$-200	24.94	65.08	4.76×10^{-3}	3.82×10^{-3}
A-$CoFe_2O_4$-300	3.79	8.40	1.49×10^{-3}	8.54×10^{-4}
A-$CoFe_2O_4$-400	2.91	6.30	5.57×10^{-4}	2.96×10^{-4}
A-$CoFe_2O_4$-500	1.01	2.08	8.09×10^{-5}	4.05×10^{-5}

decreased enormously after 5 min of contact time between the solid material and the initial solution without producing any other compound, except for the A-$CoFe_2O_4$-200 where a certain quantity of 4-NP was produced. The quantification made after 5 min revealed that 54.2%, 38.2%, 14.8%, 9.4%, 2.4% of the initial quantity of 4-NPP has been adsorbed on the surface of A-$CoFe_2O_4$-RT, A-$CoFe_2O_4$-200, A-$CoFe_2O_4$-300, A-$CoFe_2O_4$-400 and A-$CoFe_2O_4$-500, respectively. The value given for the A-$CoFe_2O_4$-200 is in reality the difference between the decreased 4-NPP concentration and the produced 4-NP concentration. Furthermore, reference 4-NP adsorption tests performed on the different catalysts showed that no adsorption of 4-NP took place even after 24 h of contact time. Thus, we consider that the 4-NP produced during the reaction exists only in the solution.

The catalytic activities of the cobalt ferrite aerogels calcined at high temperatures (600, 700, and 800 °C) did not show any catalytic activity; however, the activity of the samples calcined at lower temperatures was found to extensively rely on the calcination temperature, as shown in Fig. 3. The A-$CoFe_2O_4$-RT and A-$CoFe_2O_4$-200 samples show the highest catalytic activities, with the A-$CoFe_2O_4$-200 being the most active. On the other hand, the samples A-$CoFe_2O_4$-300 and A-$CoFe_2O_4$-400 showed very similar activities. A-$CoFe_2O_4$-500 showed a very low activity where the 4-NP was not quantifiable before 4 h of reaction time. It is worth to mention that the quantified concentration of 4-NPP after 5 min of the reaction remains constant during the reaction time, for the totality of the catalytic tests performed. This suggests that the catalytic conversion of 4-NPP to 4-NP takes place on the surface of the catalysts and the product (4-NP) is released in the solution with the 4-NPP/solid equilibrium being maintained. For that reason, the predicted 4-NPP conversion and reaction rate calculations were made according to the quantity of 4-NP present in the solution.

Table 2 regroups the calculated 4-NPP conversion taking into consideration the adsorbed quantities of 4-NPP after 5 and 24 h of reaction time, as well as the initial rate constants obtained for the different aerogels. These results show that the A-$CoFe_2O_4$-RT and A-$CoFe_2O_4$-200 are efficient catalysts for the hydrolysis of 4-nitrophenyl phosphate with 100% selectivity for 4-nitrophenol and

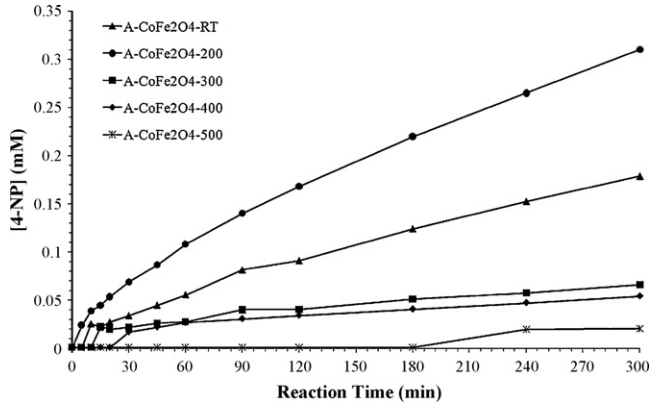

Fig. 3. Effect of the heat treatment on the conversion of 4-NPP. [4-NPP] = 2 mM; solvent volume = 25 mL; pH = 9.5; T = 30 °C; catalyst weight = 50 mg.

conversions exceeding 55% and 65% after 24 h with initial rate constants equal to 2.67×10^{-3} and 3.82×10^{-3} min^{-1}, respectively.

The correlation of the catalysis results with the FTIR spectroscopy reveals that the catalytic activity is directly related to the existence of OH surface groups. As seen in FTIR, the intensity of the OH band decreases as the annealing temperature increases, and disappears after 600 °C. The same trend was noticed for the catalytic activity, which decreases at high calcination temperatures and became null for the samples calcined at 600 °C and above. The case of the A-$CoFe_2O_4$-RT, where the OH groups are the most abundant and the corresponding band is the most intense compared to the other catalysts, is an exception to this catalytic activity-OH group correlation. Most likely, this is due to the existence of adsorbed organic groups on the large surface of the aerogel responsible of a partial inhibition of the surface OH catalytic effect.

The high porosity of the aerogels calcined at temperatures below 500 °C allows the diffusion of the 4-NPP molecules within the pores and their easy access to the surface catalytic sites where they are hydrolyzed. Conversely, the catalytic inactivity of aerogels treated at temperatures greater than 600 °C is due to the low surface area and small pore volume limiting the access of the catalytic sites, besides the absence of surface OH groups.

4. Conclusion

In summary, this study described the preparation of novel highly porous cobalt ferrite aerogels via the epoxide sol–gel method and their application in the catalysis of the hydrolysis of 4-nitrophenyl phosphate. These aerogels revealed significant catalytic properties, mainly as-synthesized and after heat treatment at 200 °C. The catalytic property of these materials is found to be essentially due to the existence of residual surface OH groups that did not undergo condensation. The XRD and N_2 adsorption measurements revealed the nano-nature of these porous cobalt ferrites where the crystallite sizes range between 6.3 and 28.1 nm.

Acknowledgements

The authors are thankful for the financial support from the University Research Board at the American University of Beirut. The authors would like to acknowledge the Central Research Science Lab (CRSL) of the Faculty of Arts and Sciences at AUB where the HPLC and XRD measurements were performed.

References

[1] H.H. Hamdeh, Z. Xia, R. Foehrweiser, B.J. McCormick, R.J. Willey, G. Busca, Journal of Applied Physics 76 (1994) 1135.
[2] M. Banerjee, N. Verma, R. Prasad, Journal of Materials Science 42 (2007) 1833.
[3] H.G. El-Shobaky, S.A.H. Ali, N.A. Hassan, Materials Science and Engineering B 143 (2007) 21.
[4] T. Liu, L. Wang, P. Yang, B. Hu, Materials Letters 62 (2008) 4056.
[5] H. Lee, J. Jung, H. Kim, Y.-M. Chung, T. Kim, S. Lee, S.-H. Oh, Y. Kim, I. Song, Catalysis Letters 124 (2008) 364.
[6] J.A. Toledo-Antonio, N. Nava, M. Martínez, X. Bokhimi, Applied Catalysis A: General 234 (2002) 137.
[7] T. Mathew, S. Shylesh, B.M. Devassy, M. Vijayaraj, C.V.V. Satyanarayana, B.S. Rao, C.S. Gopinath, Applied Catalysis A: General 273 (2004) 35.

[8] C.G. Ramankutty, S. Sugunan, B. Thomas, Journal of Molecular Catalysis A: Chemical 187 (2002) 105.
[9] M. Vijayaraj, C.S. Gopinath, Journal of Catalysis 241 (2006) 83.
[10] Z. Gu, X. Xiang, G. Fan, F. Li, The Journal of Physical Chemistry C 112 (2008) 18459.
[11] P.D. Thang, G. Rijnders, D.H.A. Blank, Journal of Magnetism and Magnetic Materials 310 (2007) 2621.
[12] Z.H. Hua, R.S. Chen, C.L. Li, S.G. Yang, M. Lu, B.X. Gu, Y.W. Du, Journal of Alloys and Compounds 427 (2007) 199.
[13] K. Maaz, A. Mumtaz, S.K. Hasanain, A. Ceylan, Journal of Magnetism and Magnetic Materials 308 (2007) 289.
[14] C.-C. Wang, I.H. Chen, C.-R. Lin, Journal of Magnetism and Magnetic Materials 304 (2006) e451.
[15] L.J. Cote, A.S. Teja, A.P. Wilkinson, Z.J. Zhang, Fluid Phase Equilibria 210 (2003) 307.
[16] E. Manova, B. Kunev, D. Paneva, I. Mitov, L. Petrov, C. Estournes, C. D'Orlean, J.-L. Rehspringer, M. Kurmoo, Chemistry of Materials 16 (2004) 5689.
[17] C.H. Yan, Z.G. Xu, F.X. Cheng, Z.M. Wang, L.D. Sun, C.S. Liao, J.T. Jia, Solid State Communications 111 (1999) 287.
[18] S. Sun, H. Zeng, D.B. Robinson, S. Raoux, P.M. Rice, S.X. Wang, G. Li, Journal of the American Chemical Society 126 (2004) 273.
[19] X. Wang, J. Zhuang, Q. Peng, Y. Li, Nature 437 (2005) 121.
[20] B.G. Toksha, S.E. Shirsath, S.M. Patange, K.M. Jadhav, Solid State Communications 147 (2008) 479.
[21] T. Meron, Y. Rosenberg, Y. Lereah, G. Markovich, Journal of Magnetism and Magnetic Materials 292 (2005) 11.
[22] I.H. Gul, A. Maqsood, Journal of Alloys and Compounds 465 (2008) 227.
[23] P. Lavela, J.L. Tirado, Journal of Power Sources 172 (2007) 379.
[24] C.J. Brinker, G.W. Scherer, Sol–Gel Science. The Physics and Chemistry of Sol–Gel Processing, Academic Press, New York, 1990.
[25] A.C. Pierre, G.M. Pajonk, Chemical Reviews, Washington, DC, United States, 102, 2002, 4243.
[26] N. Huesing, F. Schwertfeger, W. Tappert, U. Schubert, Journal of Non-Crystalline Solids 186 (1995) 37.
[27] A.E. Gash, T.M. Tillotson, J.H. Satcher Jr., L.W. Hrubesh, R.L. Simpson, Journal of Non-Crystalline Solids 285 (2001) 22.
[28] Y.P. Gao, C.N. Sisk, L.J. Hope-Weeks, Chemistry of Materials 19 (2007) 6007.
[29] C.N. Sisk, L.J. Hope-Weeks, Journal of Materials Chemistry 18 (2008) 2607.
[30] S. Brunauer, P.H. Emmett, E. Teller, Journal of the American Chemical Society 60 (1938) 309.
[31] E.P. Barrett, L.G. Joyner, P.P. Halenda, Journal of the American Chemical Society 73 (1951) 373.
[32] J. Livage, M. Henry, C. Sanchez, Progress in Solid State Chemistry 18 (1988) 259.
[33] G. Socrates, Infrared and Raman Characteristic Group frequencies: Tables and Charts, John Wiley & Sons, 2001.
[34] H. Gunzler, H.-U. Gremlich, IR Spectroscopy: An Introduction, Wiley–VCH, 2002.
[35] R. Xu, H.C. Zeng, Chemistry of Materials 15 (2003) 2040.
[36] L. Zhao, H. Zhang, Y. Xing, S. Song, S. Yu, W. Shi, X. Guo, J. Yang, Y. Lei, F. Cao, Journal of Solid State Chemistry 181 (2008) 245.
[37] V.L. Calero-DdelC, C. Rinaldi, Journal of Magnetism and Magnetic Materials 314 (2007) 60.
[38] R.D. Waldron, Physical Review 99 (1955) 1727.
[39] A.L. Patterson, Physical Review 56 (1939) 978.
[40] S. Lowell, J.E. Shields, M.A. Thomas, M. Thommes, Characterization of Porous Solids and Powders: Surface Area, Pore Size and Density, Kluwer Academic Publishers, Dordrecht, The Netherlands, 2004.